**TECHNICAL TRANSACTIONS** | **CZASOPISMO TECHNICZNE**
ELECTRICAL ENGINEERING | ELEKTROTECHNIKA
1-E/2015

KRZYSZTOF LUDWINEK*

# FEMM UTILISATION IN REPRESENTATION OF INDUCTANCE DISTRIBUTIONS IN A SALIENT POLE SYNCHRONOUS GENERATOR CIRCUITAL MODEL IN NO-LOAD STATE

# WYKORZYSTANIE FEMM DO ODWZOROWANIA ROZKŁADÓW INDUKCYJNOŚCI MODELU OBWODOWEGO GENERATORA SYNCHRONICZNEGO JAWNOBIEGUNOWEGO W STANIE BIEGU JAŁOWEGO

Abstract

This paper concerns a circuital model of a 5.5 kVA salient pole synchronous generator with damping bars, with and without the rotor skew. The paper presents an influence of the stator to rotor self and mutual inductance distribution on the induced voltages in the no-load steady state. Inductance distributions used in the circuital model are determined in the FEMM program for linear and nonlinear magnetic circuit. Simulation and experimental verification are presented.

*Keywords*: *synchronous generator*, *inductance distributions*, *induced voltages*

Streszczenie

W artykule przedstawiono wpływ rozkładów indukcyjności własnych i wzajemnych uzwojeń stojana i wirnika na indukowane napięcia w stanie biegu jałowego generatora synchronicznego jawnobiegunowego o mocy 5,5 kVA z klatką tłumiącą na wirniku bez skosu oraz ze skosem. Rozkłady indukcyjności użyte w modelu obwodowym wyznaczono w programie FEMM dla liniowego i nieliniowego obwodu magnetycznego. Przedstawiono wyniki badań symulacyjnych i eksperymentalnych.

*Słowa kluczowe*: *generator synchroniczny*, *rozkłady indukcyjności*, *indukowane napięcia*
**DOI: 10.4467/2353737XCT.15.053.3853**

* Ph.D. Eng. Krzysztof Ludwinek, Department of Electrical Machines and Mechatronic Systems, Kielce University of Technology.

## 1. Introduction

Both for a designer and a user, knowing about the harmonic contents of waveforms of induced voltages in the stator winding, a synchronous generator in the no-load and load steady states is very important [1–4]. Generator sets consume more fuel due to the presence of higher harmonic contents in the induced stator voltage and current waveforms. This has negative economic consequences.

In a no-load state, a magnetic flux density in the air gap of a synchronous generator is distorted due to: the influence of the stator and rotor slot opening [5]; the presence of the damping circuits [6]; saturation of the magnetic circuit (mainly low order odd harmonics) [7, 8]; magnetic rotor asymmetry; static and dynamic stator;rotor eccentricity; inside asymmetry [9–13]. Low power salient pole synchronous generators without the rotor (or stator) skew up to several kVA due to a single-layer stator winding have the largest content of higher harmonics (in low power synchronous generators less than 10 kVA dominate single layer windings) [14–19]. No rotor skew and the presence of single-layer stator winding causes a significant increase in higher harmonic order in self and mutual inductance distributions in circuital models of synchronous generators [14–19]. In cases of powering various types of sensitive loads (e.g. UPS, PC computers, notebooks, compact fluorescent lamps and different types of audio-video electronic equipment) the induced stator voltages and the armature currents are very distorted. This case is illustrated in Figure 1, where the comparison of registered waveforms of induced stator voltages $u_a$ and $u_b$, field voltage $U_f$ and current $i_f$ in no load state for two salient pole synchronous generators with single-layer stator winding with and without the rotor skew are presented. The first generator rated data as follows: $S_N$ = 5.5 VA; $U_N$ = 400 V (*Y*); $I_N$ = 7.9 A; cosφ$_N$ = 0.8; $n_N$ = 3000 rpm; $Q_s$ = 24, $p$ = 1 (number of pole pairs); $\alpha_q$ = 15° (angle of rotor skew). The second generator rated data as follows: $S_N$ = 10 kVA; $U_N$ = 400 V (*Y*); $I_N$ = 14.5 A; cosφ$_N$ = 0.8, $n_N$ = 3000 rpm; $Q_s$ = 24, $p$ = 1, $\alpha_q$ = 0° (without the rotor skew). During the investigations, field winding is powered by a DC voltage source ($U_f$ = const.).

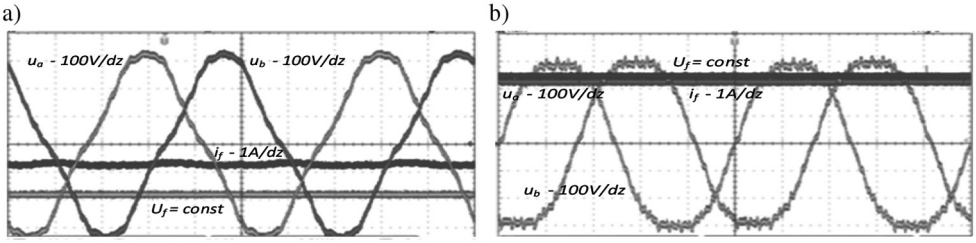


Fig. 1. Comparison of registered induced stator voltages in no load state for two salient pole synchronous generators: a) with the rotor skew, b) without the rotor skew

The total harmonic distortion ($THDu_a$) counted up to the 100$^{th}$ harmonic in the presented waveforms (in Fig. 1) of the induced phase voltages under no-load conditions are [18]:

- with the rotor skew $THDu_{as}$ = 8.41%,
- without the rotor skew $THDu_a$ = 10.21%.

The participation of the higher harmonics in the induced stator voltages is the most visible during the powering of sensitive receivers. The two synchronous generators (with and without the rotor skew) are used for powering a PC set-up (a PC unit, a monitor and a laser jet printer). In Figure 2, comparison of registered waveforms of the distorted load current $i_a$ for the two salient pole synchronous generators with and without the rotor skew are presented. During the investigation, the field winding is powered by a DC voltage source ($U_f$ = const.).

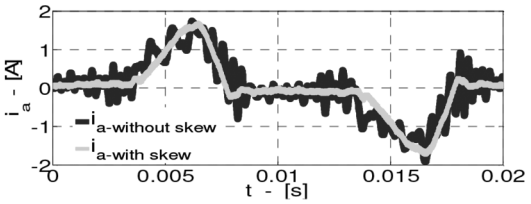


Fig. 2. Comparison of currents of two synchronous generators with and without the rotor skew

In Figure 3, the comparison of load current magnitudes with and without the rotor skew (Fig. 2) due to the Fourier analysis is presented.

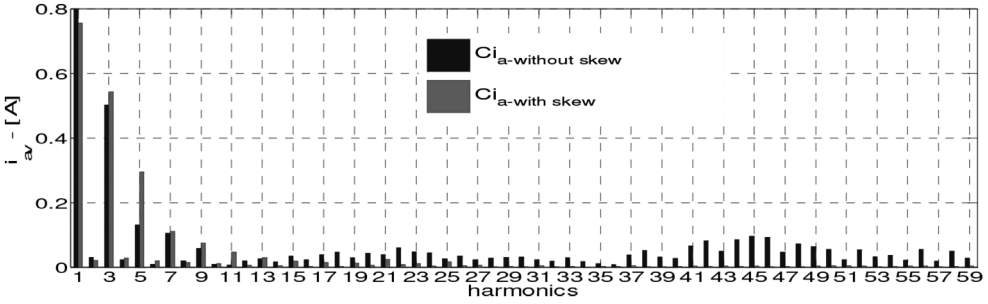


Fig. 3. Comparison of current magnitude harmonics

The total harmonic distortion counted up to the 100th harmonic in the presented waveforms (in Fig. 2) during powering the PC set-up are:

- with the rotor skew $THDi_{as}$ = 80.14%,
- without the rotor skew $THDi_a$ = 84.21%.

Although, from the 14th harmonic the higher harmonic contents are greater for the 10 kVA synchronous generator (without the rotor skew) than for the 5.5 kVA version (with the rotor skew) due to saturation of the magnetic circuit (mainly 3rd and 5th harmonics Figs. 2 and 3 and lower fundamental magnitude for generator with the rotor skew than without the rotor skew), the total harmonic distortion for the synchronous generator with the rotor skew $THDi_{as}$ is equal to 80.14%. It is similar to $THDi_a$ = 84.21% (for the synchronous generator without the rotor skew). In the presented waveforms (in Fig. 2), the harmonic contents can be calculated by the Telephone Harmonic Factor $THFi_a$ (from 14th to the 100th harmonic):

- with the rotor skew $THFi_{as}$ = 44.21%,
- without the rotor skew $THFi_{a}$ = 6.22%.

From presented Figs. 1–3 results, that about a better quality of synchronous generator can decide the harmonic contents in induced stator voltages in the no-load state.

The most important aspect in simulations using a circuital model of a synchronous generator is choosing suitable reference frames and the presence of the damping circuits [5, 6, 8–10, 14–17]. Studies of synchronous generators using circuital models are very popular in the rotor reference frame $dq0$ due to constant inductance distributions. But this assumption (constant inductance distributions) is true if the self and mutual inductances of the stator windings contain only the constant component and the same magnitude of the 2nd harmonic [19]. As shown in [19], for linear and nonlinear magnetic circuit the Park's transformation of the higher harmonics of the stator self and mutual inductance distributions to the $dq0$-axes introduces only additional unnecessary calculations (because not only the self inductance distributions in the $dq0$-axes but also the mutual ones contain higher harmonics) [19].

This paper presents an influence of the stator to rotor self and mutual inductance and derivative distributions on the waveforms of induced phase stator voltages in the no-load steady state of the nonlinear 5.5 kVA salient pole synchronous generator with damping bars on the rotor with and without the skew. In the circuital model, the self and mutual inductance distributions are obtaind using the FEMM program. Detailed analysis of the influence of the rotor skew on the reduction of higher harmonics in self and mutual inductances are presented in [14–19].

## 2. Model of a salient pole synchronous generator in the stator and rotor natural reference frame

Due to contents of higher harmonics in the self and mutual inductance distributions in the $dq0$-axes, simulations of the induced phase stator voltages $u_a$, $u_b$ and $u_c$ with a circuital model of a salient pole synchronous generator is easier to carry out in the stator and the rotor natural reference frame [19]. In Figure 4, the equivalent circuit parameters of a salient pole synchronous generator in the no-load state are presented [17].

The circuit model (Fig. 4) consists of the field winding, three phase stator windings ($i_a$, $i_b$ and $i_c$ are equal to 0) and damping bars (5 bars per pole) with segment of rings. On differential linkage fluxes in no-load state have the influence the electrical angle of the rotor position θ, the field current ($i_f$) and currents in the equivalent 10 damping bars and ring segments ($i_{r(1)}$, ..., $i_{r(10)}$). As shown in [14], the amplitudes of higher harmonic currents $i_{r(1)v}$, ..., $i_{r(10)v}$ in the no-load steady state of the 5.5 kVA salient pole synchronous generator are very small. In this condition, on the magnetic flux distribution the field winding ampere-conductors have significant influence and the damping bar ampere-conductors can be omitted. So, in the no-load steady state it can be assumed that on the self and mutual inductance distributions have influence only the electrical angle of the rotor position θ and field current $i_f$.

In the circuital model (Fig. 4), the induced stator phase voltages $u_a$, $u_b$, $u_c$, the field voltage $u_f$ and the induced voltage in the $k$-th shorted equivalent damping bar can be expressed as [17]:

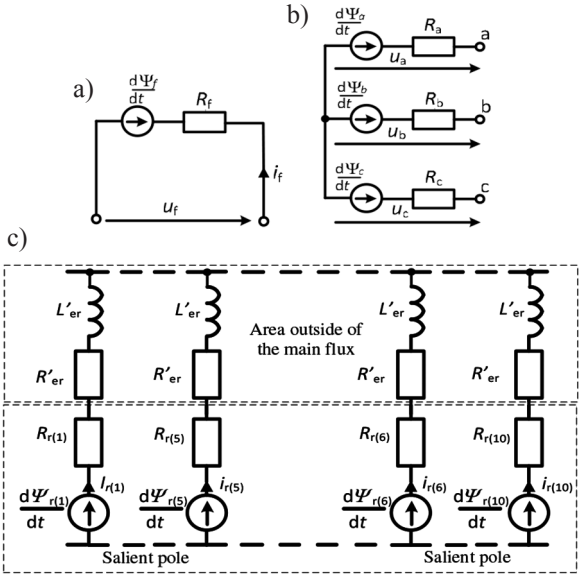


Fig. 4. Equivalent circuit parameters of a salient pole synchronous generator in the stator and rotor natural reference frame a) field winding, b) stator windings, c) damping circuits

$$\frac{\mathrm{d}\psi_a(\theta,i_f)}{\mathrm{d}t}=u_a,\quad \frac{\mathrm{d}\psi_b(\theta,i_f)}{\mathrm{d}t}=u_b,\quad \frac{\mathrm{d}\psi_c(\theta,i_f)}{\mathrm{d}t}=u_c \tag{1}$$

$$\frac{\mathrm{d}\psi_f(\theta,i_f)}{\mathrm{d}t}+R_f i_f=u_f \tag{2}$$

$$\frac{\mathrm{d}\psi_{r(k)}(\theta,i_f)}{\mathrm{d}t}+R_{r(k)}i_{r(k)}+L_{er}\frac{i_{r(k)}}{\mathrm{d}t}=0 \tag{3}$$

$$\frac{\mathrm{d}\theta}{\mathrm{d}t}=p\omega \quad \text{and} \quad i_{r(1)}+i_{r(2)}+\ldots+i_{r(k)}=0 \tag{4}$$

where:

$a, b, c, f$ – indexes of stator windings and field winding,
$\Psi_a, \Psi_b, \Psi_c, \Psi_f$ – stator and field winding linkage fluxes,
$u_a, u_b, u_c, u_f$ – stator phase voltages and field voltage,
$R_f$ – resistance of the field winding,
$i_f$ – field current,
$r(k)$ – index of $k$-th-damping bar $k = \{1, 2, \ldots, 10\}$,
$\Psi_{r(k)}$ – $k$-th damping bar linkage flux,
$R_{r(k)}$ – resistance of equivalent damping bar and ring elements.

$$R_{r(k)} = R_{pr} + R_{er}/\{2\sin^2(\alpha_{(k)})\} = R_{pr} + R'_{er},$$

$R_{pr}$, $R'_{er}$ – resistance of damping bar (in area of main flux) and equivalent ring elements (in area outside of main flux),
$\alpha_{(k)}$ – an angle between the equivalent $k$-th rotor damping bar (with ring elements) and the rotor reference axis, $\alpha_{(k)} = p\pi/Q_r$,
$Q_r$ – number of rotor bars,
$L'_{er}$ – equivalent inductance of end ring elements, $L'_{er} = L_{er}/\{2\sin^2(\alpha_{(k)})\}$,
$i_{r(k)}$ – current in $k$-th damping bars and ring elements,
$\theta$ – electrical angle of the rotor position $\theta = \theta_m p$,
$\theta_m$ – mechanical angle of the rotor position,
$\omega$ – electrical angular velocity $\omega = (1/p)\cdot d\theta/dt$.

The differential linkage fluxes can be derived from the following equations:

$$\frac{\mathrm{d}\boldsymbol{\psi}_{sfr}(\theta, i_f)}{\mathrm{d}t} = \frac{\mathrm{d}\theta}{\mathrm{d}t}\frac{\partial \mathbf{L}_{sfr}(\theta,\ i_f)}{\partial\theta}\mathbf{i}_{sfr} + \mathbf{L}_{sfr}(\theta,\ i_f)\frac{\mathrm{d}\mathbf{i}_{sfr}}{\mathrm{d}t} \tag{5}$$

where:
$\mathbf{i}_{sfr}$ – matrix of the stator currents (equal to zero), field current and currents in the equivalent 10 damping bars and ring elements $[0, 0, 0, i_f, i_{r(1)}, \ldots, i_{r(10)}]^T$,
$\boldsymbol{\Psi}_{sfr}$ – matrix of linkage fluxes of stator windings, field winding, and equivalent 10 damping bars $[\Psi_a, \Psi_b, \Psi_c, \Psi_f, \Psi_{r(1)}, \ldots, \Psi_{r(10)}]^T$, whereas $\boldsymbol{\Psi}_{sfr} = \mathbf{L}_{sfr}\mathbf{i}_{sfr}$,
$\mathbf{L}_{sfr}$ – matrix of self and mutual inductances of stator-to-rotor windings and damping bars (and ring elements) can be expressed as:

$$\mathbf{L}_{sfr}(\theta,\ i_f) = \begin{bmatrix}
L_a + L_{es} & L_{ab} & L_{ac} & L_{af}(\theta,\ i_f) & L_{ar(1)}(\theta,\ i_f) & \ldots & L_{ar(10)}(\theta,\ i_f) \\
L_{ba} & L_b + L_{es} & L_{bc} & L_{bf}(\theta,\ i_f) & L_{br(1)}(\theta,\ i_f) & \ldots & L_{br(10)}(\theta,\ i_f) \\
L_{ca} & L_{cb} & L_c + L_{es} & L_{cf}(\theta,\ i_f) & L_{cr(1)}(\theta,\ i_f) & \ldots & L_{cr(10)}(\theta,\ i_f) \\
L_{fa}(\theta,\ i_f) & L_{fb}(\theta,\ i_f) & L_{fc}(\theta,\ i_f) & L_f(\theta,\ i_f) + L_{ef} & L_{fr(1)}(\theta,\ i_f) & \ldots & L_{fr(10)}(\theta,\ i_f) \\
L_{r(1)a}(\theta,\ i_f) & L_{r(1)b}(\theta,\ i_f) & L_{r(1)c}(\theta,\ i_f) & L_{r(1)f}(\theta,\ i_f) & L_{r(1)}(\theta,\ i_f) + L_{er} & \ldots & L_{r(1,10)}(\theta,\ i_f) \\
\ldots & \ldots & \ldots & \ldots & \ldots & \ldots & \ldots \\
L_{r(10)a}(\theta,\ i_f) & L_{r(10)b}(\theta,\ i_f) & L_{r(10)c}(\theta,\ i_f) & L_{r(10)f}(\theta,\ i_f) & L_{r(10,1)}(\theta,\ i_f) & \ldots & L_{r(10)}(\theta,\ i_f) + L_{er}
\end{bmatrix}$$

where:
$L_{af}$, $L_{bf}$, $L_{cf}$ – mutual inductance of the stator windings to the field winding ($L_{fa}$, $L_{fb}$, $L_{fc}$),
$L_{ar(k)}$, $L_{br(k)}$, $L_{cr(k)}$ – mutual inductance of the stator windings to $k$-th damping bar and ring element ($L_{r(k)a}$, $L_{r(k)b}$, $L_{r(k)c}$),
$L_f$ – self inductance of the field winding,
$L_{fr(k)}$ – mutual inductance of the field winding to $k$-th damping bar and ring element ($L_{r(k)f}$),
$L_{r(k)}$ – self inductance of $k$-th damping bar and ring element,
$L_{es}$, $L_{ef}$, $L_{er}$ – leakage inductance of stator winding, field winding and ring element.

From relations (1) to (5) in the no-load state, the matrix describing induced stator voltages whilst taking into account 10 damping bars with the ring segments can be expressed as [17]

$$\begin{bmatrix} u_a \\ u_b \\ u_c \end{bmatrix} = \omega \frac{\partial}{\partial \theta} \begin{bmatrix} L_{af}(\theta,\, i_f) & L_{ar(1)}(\theta,\, i_f) & \ldots & L_{ar(10)}(\theta,\, i_f) \\ L_{bf}(\theta,\, i_f) & L_{br(1)}(\theta,\, i_f) & \ldots & L_{br(10)}(\theta,\, i_f) \\ L_{cf}(\theta,\, i_f) & L_{cr(1)}(\theta,\, i_f) & \ldots & L_{cr(10)}(\theta,\, i_f) \end{bmatrix} \begin{bmatrix} i_f \\ i_{r(1)} \\ \ldots \\ i_{r(10)} \end{bmatrix} + \begin{bmatrix} L_{af}(\theta,\, i_f) & L_{ar(1)}(\theta,\, i_f) & \ldots & L_{ar(10)}(\theta,\, i_f) \\ L_{bf}(\theta,\, i_f) & L_{br(1)}(\theta,\, i_f) & \ldots & L_{br(10)}(\theta,\, i_f) \\ L_{cf}(\theta,\, i_f) & L_{cr(1)}(\theta,\, i_f) & \ldots & L_{cr(10)}(\theta,\, i_f) \end{bmatrix} \frac{\mathrm{d}}{\mathrm{d}t} \begin{bmatrix} i_f \\ i_{r(1)} \\ \ldots \\ i_{r(10)} \end{bmatrix} \tag{6}$$

From relations (1) to (5) in the no-load state, the matrix describing circuits of the field winding and the equivalent 10 damping bars with the ring segments can be expressed as:

$$\begin{bmatrix} u_f \\ 0 \\ \ldots \\ 0 \end{bmatrix} = \left\{ \omega \frac{\partial}{\partial \theta} \begin{bmatrix} L_f(\theta,\, i_f) + L_{ef} & L_{fr(1)}(\theta,\, i_f) & \ldots & L_{fr(10)}(\theta,\, i_f) \\ L_{r(1)f}(\theta,\, i_f) & L_{r(1)}(\theta,\, i_f) + L_{er} & \ldots & L_{r(1,10)}(\theta,\, i_f) \\ \ldots & \ldots & \ldots & \ldots \\ L_{r(10)f}(\theta,\, i_f) & L_{r(1,10)}(\theta,\, i_f) & \ldots & L_{r(10)}(\theta,\, i_f) + L_{er} \end{bmatrix} + \begin{bmatrix} R_f & 0 & \ldots & 0 \\ 0 & R_{r(1)} & \ldots & 0 \\ \ldots & \ldots & \ldots & \ldots \\ 0 & 0 & \ldots & R_{r(10)} \end{bmatrix} \right\} \begin{bmatrix} i_f \\ i_{r(1)} \\ \ldots \\ i_{r(10)} \end{bmatrix} +$$

$$+ \begin{bmatrix} L_f(\theta,\, i_f) + L_{ef} & L_{fr(1)}(\theta,\, i_f) & \ldots & L_{fr(10)}(\theta,\, i_f) \\ L_{r(1)f}(\theta,\, i_f) & L_{r(1)}(\theta,\, i_f) + L_{er} & \ldots & L_{r(1,10)}(\theta,\, i_f) \\ \ldots & \ldots & \ldots & \ldots \\ L_{r(10)f}(\theta,\, i_f) & L_{r(1,10)}(\theta,\, i_f) & \ldots & L_{r(10)}(\theta,\, i_f) + L_{er} \end{bmatrix} \frac{\mathrm{d}}{\mathrm{d}\square} \begin{bmatrix} i_f \\ i_{r(\square)} \\ \ldots \\ i_{r(\square 0)} \end{bmatrix} \tag{7}$$

In expression (7), the significant simplification of the description of the model (in relation to classical circuit model) is the diagonal matrix of resistance (of field winding and damping bars with ring segments).

### 3. Determination of the self and mutual inductance distributions

Figure 5 presents magnetic flux distribution lines obtained using the FEMM program [11–14] for the examined nonlinear 5.5 kVA salient pole synchronous generator (with and without the rotor skew with shorted 10 equivalent damping bars) rated: $S_N$ = 5.5 kVA; $U_N$ = 400 V (*Y*); $n_N$ = 3000 rpm; $I_N$ = 7.9 A; cos$\varphi_N$ = 0.8; $p$ = 1; $Q_s$ = 24; $\alpha_q$ = 15° (factory rotor skew equal to stator slot pitch). In FEMM software, the magnetic field distribution (Fig. 5) and inductance distributions are obtained from current flowing in the field winding (in Fig. 5, two upper and two lower slots on the rotor) as a function of the electrical rotor position an-

gle θ. The calculations are carried out on the basis of the real construction data of the 5.5 kVA synchronous generator in the no load steady state with initial rotor position $\theta_0 = 0$ (Fig. 5). A method of determining the self and mutual inductance distributions in FEMM program is presented in [17].

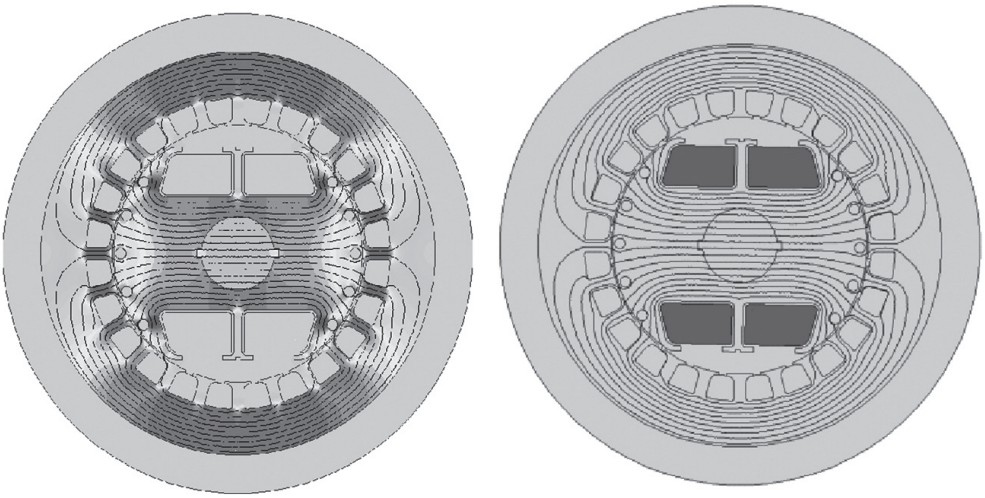

Fig. 5. Distribution lines in the 5.5 kVA salient pole synchronous generator with 10 damping bars in the no-load state a) magnetic flux density, b) current density in the field winding

In the induced stator voltages (6) in the no-load state, one of the most important are stator to field winding inductance distributions. The fundamental components of the induced stator voltages $u_{a1}$, $u_{b1}$, $u_{c1}$ are the products of electrical angular velocity ω and mutual inductance derivative distributions ($\partial L_{af1}/\partial\theta$), $\partial L_{bf1}/\partial\theta$), $\partial L_{cf1}/\partial\theta$)) and constant component of the field current $i_{f0}$. Each phase stator winding gives the product $u_{a1} = \omega(\partial L_{af1}/\partial\theta)i_{f0}$, $u_{b1} = \omega(\partial L_{bf1}/\partial\theta)i_{f0}$, and $u_c = \omega(\partial L_{af1}/\partial\theta)i_{f0}$. In the case of winding, symmetry the voltage magnitudes are equal.

Figures 6–12 contain the next indicates: *s* – index with the rotor skew; *n* – index for nonlinear model. Figure 6 shows the comparison of the stator to field winding mutual distributions for the nonlinear model without the rotor skew ($L_{af}$). In the case of the nonlinear model, the influence of saturation on the inductance distribution for better visibility is presented from 120° to 240° (Fig. 6b)). The mutual inductance distribution for the nonlinear model with the rotor skew (Fig. 6) is very similar to the model without the rotor skew. The differences are only visible after calculation of the product $\omega\partial L_{afsn}/\partial\theta$ and $\omega\partial L_{afn}/\partial\theta$ (nonlinear model with and without the rotor skew – Fig. 7a)) or the product $\omega\partial L_{afsn}/\partial\theta$ and $\omega\partial L_{afn}/\partial\theta$ in relation to $\omega\partial L_{af1}/\partial\theta$ (fundamental component of linear model – Fig. 7b)) and in higher harmonic contents due to the Fourier analysis (Fig. 8). In Figure 8c), higher harmonic contents from $65^{th}$ to $75^{th}$ (in the zoom window from 0 to 1%) are presented.

Figure 9 shows the comparison of the mutual stator to damping bars (5 damping bars per pole) inductance and the inductance derivative distributions without the rotor skew (in relation to the linear one) and higher harmonic contents due to the Fourier analysis (Fig. 10).

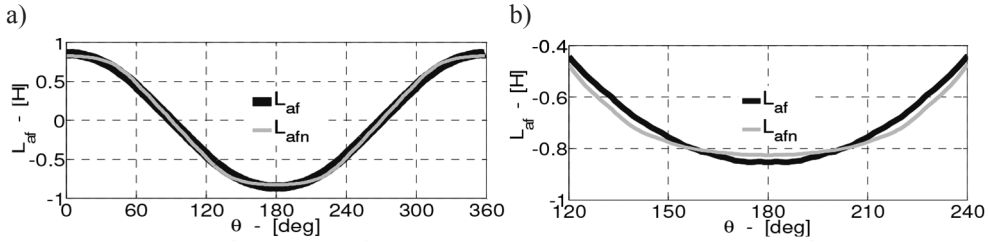


Fig. 6. Comparison of the stator to field winding mutual inductance distributions for the linear and nonlinear model without the rotor skew $L_{af}$ and $L_{afn}$ a) θ = 0°–360°, b) θ =120°–240°

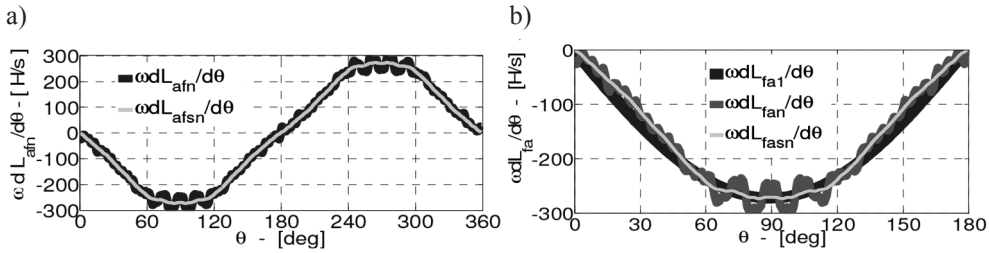


Fig. 7. Comparison of the stator to field winding mutual distributions of the product a) $\omega\partial L_{afn}/\partial\theta$ and $\omega\partial L_{afsn}/\partial\theta$, b) $\omega\partial L_{af1}/\partial\theta$, $\omega\partial L_{afn}/\partial\theta$, and $\omega\partial L_{afsn}/\partial\theta$ (in zoom window from θ = 0° to θ = 180°)

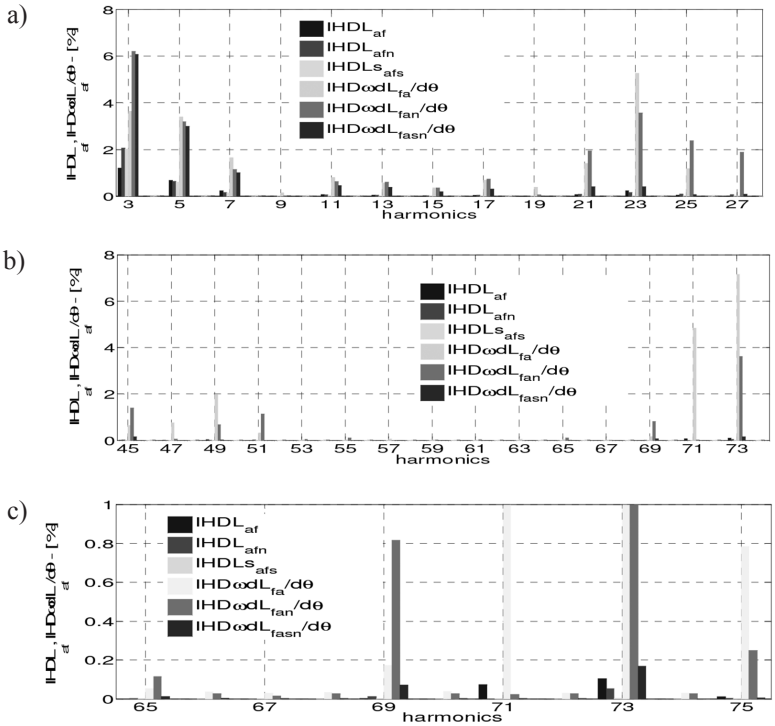


Fig. 8. Comparison of harmonic contents of the stator to field winding mutual inductance and inductance derivative distributions a) from 3rd to 29th, b) from 39th to 63th, c) from 65th to 75th

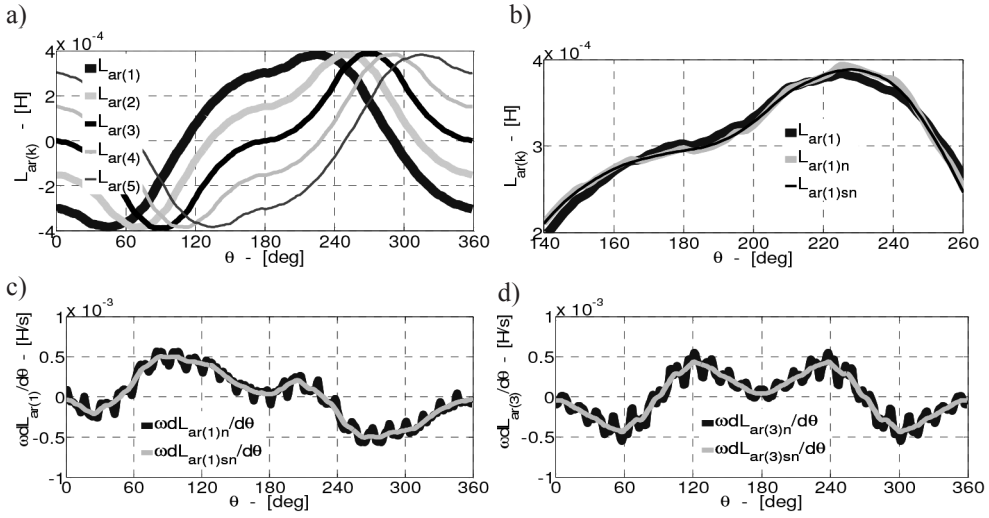


Fig. 9. Comparison of the mutual stator to damping bar inductance and the inductance derivative distributions for the linear and nonlinear model a) $L_{ar(1)}$ - $L_{ar(5)}$, b) $L_{ar(1)}$, $L_{ar(1)n}$, and $L_{ar(1)sn}$ (in zoom window from θ = 140° to θ = 260° for better visibility), c) products of $\omega\partial L_{ar(1)n}/\partial\theta$ and $\omega\partial L_{ar(1)sn}/\partial\theta$, d) products of $\omega\partial L_{ar(3)n}/\partial\theta$ and $\omega\partial L_{ar(3)sn}/\partial\theta$

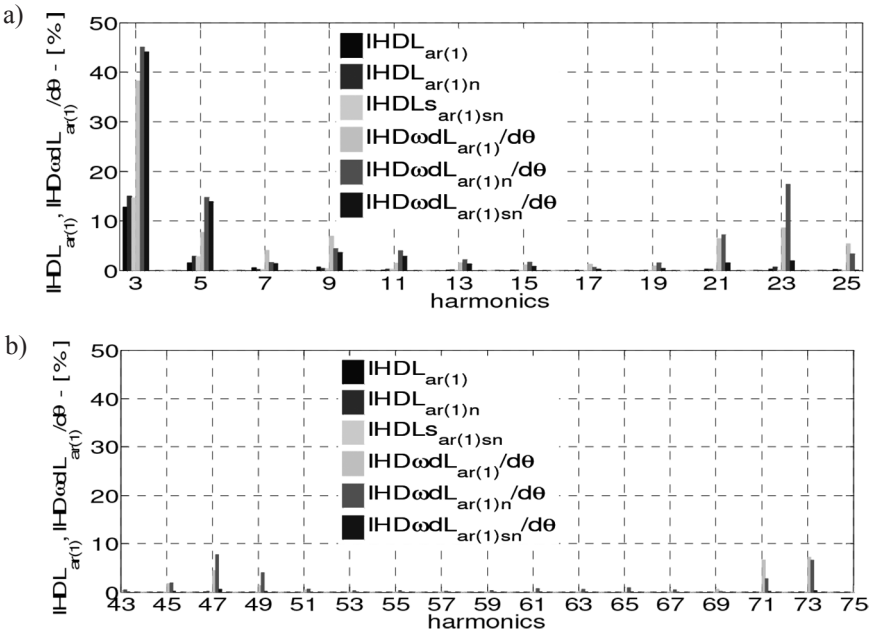


Fig. 10. Comparison of harmonic contents of the stator to damping bar mutual inductance and inductance derivative distributions of a) from 3rd to 25th, b) from 43rd to 75th

In the harmonic spectrum comparison of the mutual inductance and the inductance derivative distributions (Figs. 8 and 10), it can be seen that odd harmonics dominate. The greatest reduction of the higher harmonic order is achieved by the rotor skew. From the harmonic spectrum comparison results, it can be seen that for the examined 5.5 kVA salient pole synchronous generator without the rotor skew, the participation of, for example, the 73rd harmonic of the stator to field winding mutual inductance distribution is very small and is only 0.1% (with relation to the fundamental component Fig. 8c)). In the case of calculating the mutual inductance derivative (Fig. 8), the value is enhanced 73 times by the derivative order value and the participation increases to 7.3% (with respect to the derivative fundamental component). Similarly, the participation of the other higher harmonics that are the most visible in the inductance distributions (Figs. 8 and 10) are enhanced by the derivative order value [16].

In the case of the mutual inductance and the inductance derivative distributions of the stator to rotor damping bar with and without the rotor skew, the most significant is the 3rd harmonic. A skew of the rotor has a significant influence on the reduction in higher-order harmonic [16–19]. So, the lower-order harmonics (for example, caused by the saturation of the magnetic circuit) are only slightly reduced due to the rotor skew (Figs. 8 and 10).

As shown in [15], the field current (7) depends on the method of powering the field winding. Moreover, the field current and currents in 10 damping bars depend on the self and mutual rotor inductance and inductance derivative distributions (7). Figure 11 shows the comparison of the field winding self inductance and the inductance derivative distributions without the rotor skew and higher harmonic contents due to the Fourier analysis.

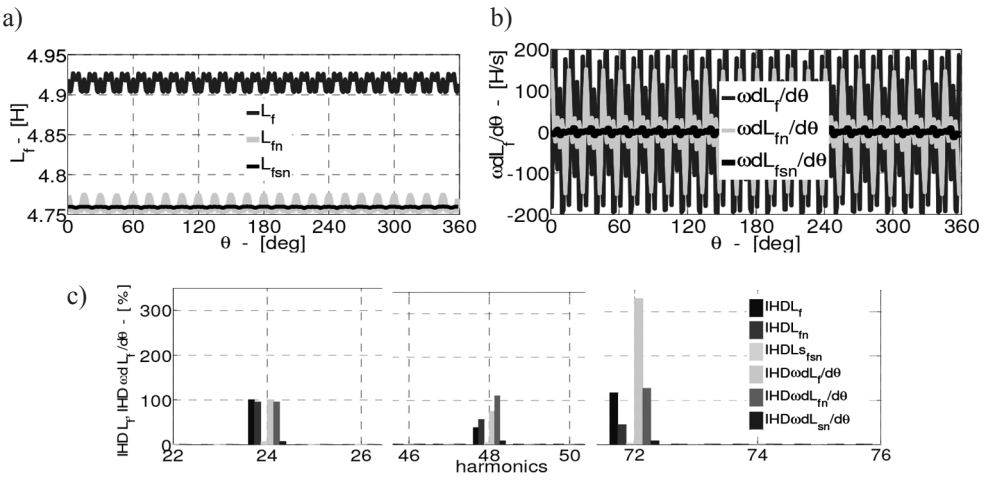


Fig. 11. Comparison of the field winding a) self inductance distributions for linear and nonlinear model, b) products of ω($\partial L_f/\partial\theta$), ω($\partial L_{fn}/\partial\theta$) and ω($\partial L_{fsn}/\partial\theta$), c) detailed harmonic contents of the inductance and inductance derivative distributions for 24th, 48th and 72nd order

In Figure 12, the comparison of the field winding to damping bars mutual inductance distributions $L_{fr(1)n}$ - $L_{fr(5)n}$ ($L_{fr(6)n}$ - $L_{fr(10)n}$), the product of ω($\partial L_{fr(1)sn}/\partial\theta$) and ω($\partial L_{fr(1)n}/\partial\theta$) for nonlinear model (with and without the rotor skew) and the harmonic contents in relation to the constant component of $L_{fr(0)}$ due to the Fourier analysis are presented. The differences be-

tween $L_{fr(1)} - L_{fr(5)}$ ($L_{fr(6)} - L_{fr(10)}$) and $L_{fr(1)n} - L_{fr(5)n}$ ($L_{fr(6)n} - L_{fr(10)n}$) for linear and nonlinear models are very small and therefore, in Fig. 12, is shown only the nonlinear model.

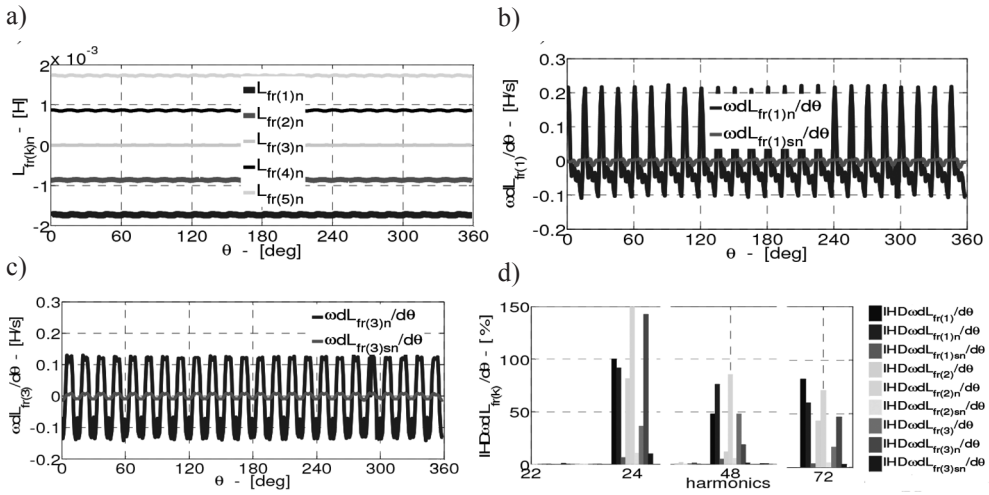


Fig. 12. Distributions of a) the field winding to damping bars mutual inductance, b) products $\omega(\partial L_{fr(1)n}/\partial\theta)$ and $\omega(\partial L_{fr(1)sn}/\partial\theta)$, c) products $\omega(\partial L_{fr(3)n}/\partial\theta)$ and $\omega(\partial L_{fr(3)sn}/\partial\theta)$, d) harmonic contents

## 4. Numerical simulations using the circuital model

**S**imulation studies of the influence of the DC voltage powering the field winding on higher harmonic contents in the induced stator phase voltages and the field and damping bar currents under no-load steady state conditions for the examined 5.5 kVA salient pole synchronous generator with and without the rotor skew are obtaind using the circuital model – expressions (6) and (7). Figure 13 shows the transient state of currents in 5 damping bars (per pole) after switching on the DC voltage that is powering the field winding.

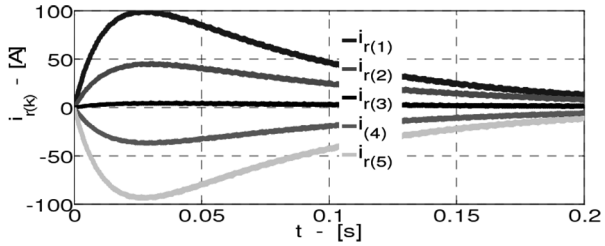


Fig. 13. Transient state of currents in 5 damping bars

Presented in Figs. 14–16, waveforms and harmonic contents are obtaind in an almost steady state. Figure 14 shows current waveforms $i_{r(1)}$ (without the rotor skew) and $i_{r(1)s}$ (with the rotor skew), the current derivatives $\mathrm{d}i_{r(1)}/\mathrm{d}t$ and $\mathrm{d}i_{r(1)s}/\mathrm{d}t$ and harmonic contents due to the Fourier analysis of the nonlinear model.

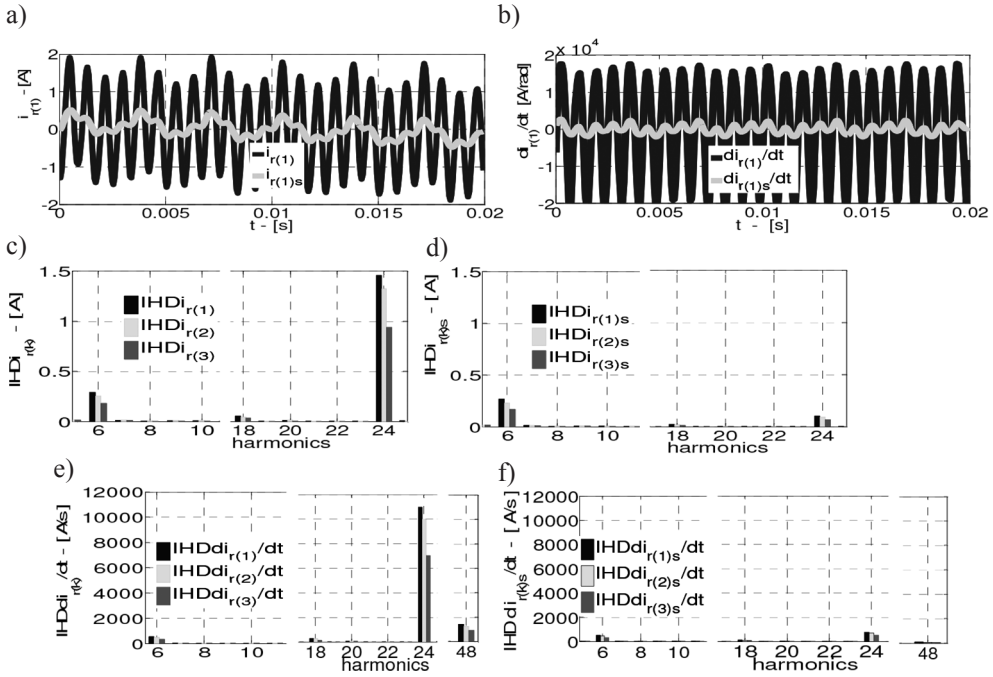


Fig. 14. Comparison of a) the currents $i_{r(1)}$ and $i_{r(1)s}$, b) the derivatives d$i_{r(1)}$/d$t$ and d$i_{r(1)s}$/d$t$, c) and d) and e) and f) harmonic contents of $i_{r(1),}$ $i_{r(2)}$, $i_{r(3)}$ and $i_{r(1)s}$, $i_{r(2)s}$, $i_{r(3)s}$, d$i_{r(1)}$/d$t$, d$i_{r(2)}$/d$t$, d$i_{r(3)}$/d$t$ and d$i_{r(1)s}$/d$t$, d$i_{r(2)s}$/d$t$, d$i_{r(3)s}$/d$t$

Figure 15 shows current waveforms $i_f$ (without the rotor skew) and $i_{fs}$ (with the rotor skew), the current derivatives d$i_f$/d$t$ and $di_{fs}/dt$ and harmonic contents due to the Fourier analysis.

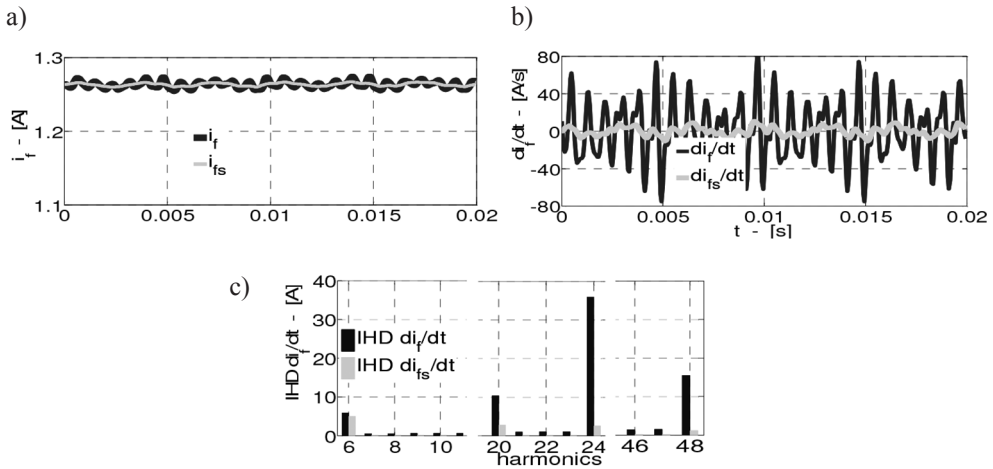


Fig. 15. Comparison of a) current waveforms $i_f$ and $i_{fs}$, b) derivatives d$i_f$/d$t$ and d$i_f$/d$t$, c) harmonic contents

As shown in Figs. 14 and 15, due to the presence of the $Q_s = 24$ open stator slots in some damping bars on the rotor $k = \{1, 5, 6, 10\}$ the current derivative $\mathrm{d}\mathbf{i}_{r(k)}/\mathrm{d}t$ for the 24th harmonic has a value of almost 11 kA/s. Moreover, the current derivative $\mathrm{d}\mathbf{i}_f/\mathrm{d}t$ for the same harmonic has a value of almost 36 A/s. This implies in the circuital model that in (6), the product of the stator to rotor mutual inductance distributions and rotor current derivatives (in the model without the rotor skew) have a significant impact on induced stator voltages in the no-load state. For the model with the rotor skew in the waveform of the rotor current derivatives dominate the low order 6th harmonic because the 24th harmonic is reduced due to the rotor skew.

Figure 16 shows the simulation of the induced stator phase voltage waveforms $u_{as}$, $u_{bs}$, and $u_{cs}$ and $u_a$, $u_b$, and $u_c$ (with and without the rotor skew) when the DC voltage is powering the field winding of the examined nonlinear 5.5 kVA synchronous generator. Moreover, in Fig. 16, the contents of harmonic magnitudes due to the Fourier analysis are presented.

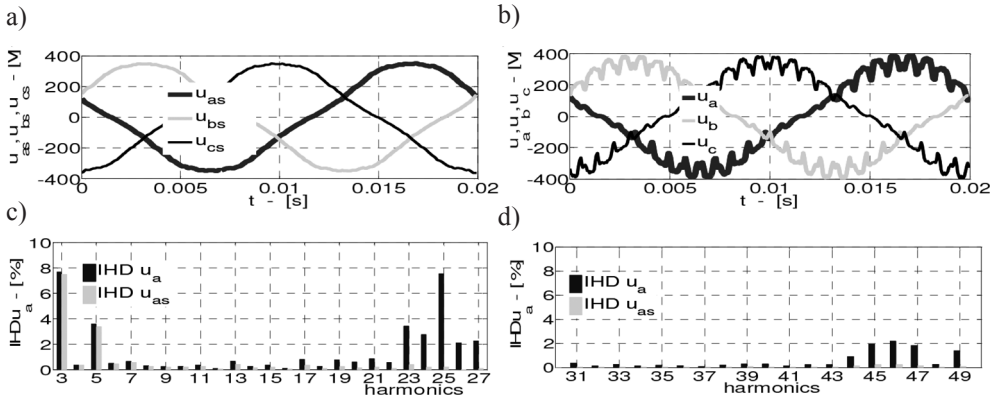


Fig. 16. Induced stator phase voltages under no-load conditions ($U_f$ = const.) a) waveforms for model with the rotor skew, b) waveforms for model without the rotor skew, c) and d) harmonic contents

In the presented waveforms (in Fig. 16), the total harmonic distortion $THDu_a$ for the case of $U_f$ = const. are:

- for the model with the rotor skew $THDu_{as} = 8.39\%$,
- for the model without the rotor skew $THDu_a = 13.73\%$.

## 5. Experimental verification

Figure 17 shows a measurement set for investigation of the 5.5 kVA salient pole synchronous generator with and without the rotor skew with single layer stator windings. Experimental verifications of the induced stator phase voltages are performed for the three-phase salient pole synchronous generators with the following rated data: $S_N = 5.5$ kVA; $U_N = 400$ V ($Y$); $I_N = 7.9$ A; $\cos\varphi_N = 0.8$; $n_N = 3000$ rpm; $Q_s = 24$; $p = 1$; $\alpha_q = 0°$; $\alpha_q = 15°$ (with and without the rotor skew). During the investigations, the field winding is powered by a DC voltage source. The induced stator voltages are registered using a four-channel digital oscilloscope.

Figure 18 shows registered waveforms of the induced stator phase voltages under no-load conditions.

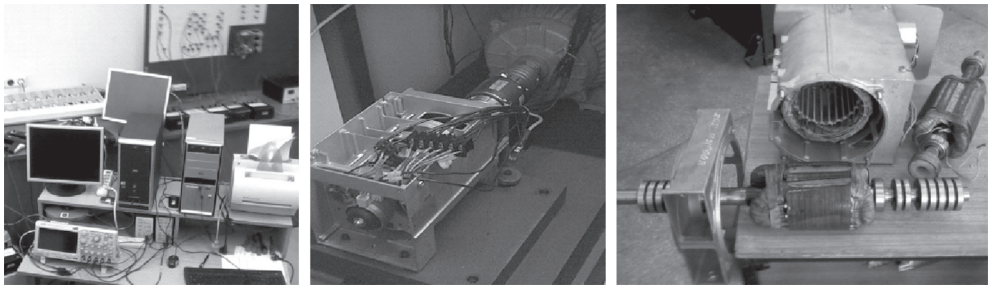

Fig. 17. Measurement set for investigation of the induced stator voltages of the 5.5 kVA salient pole synchronous generator with and without the rotor skew

a) b)

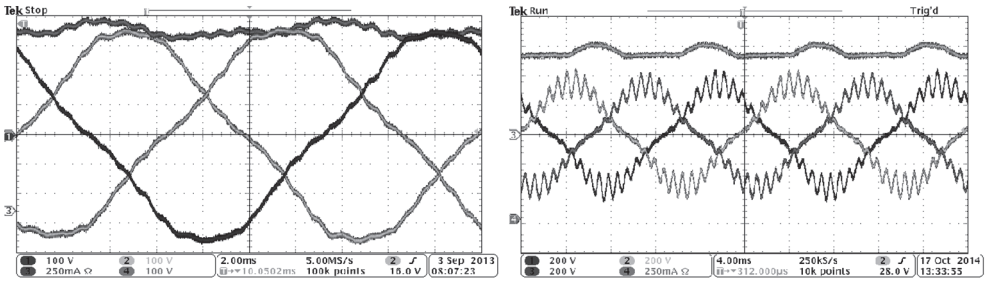


Fig. 18. Registered waveforms of the induced stator phase voltages under no-load conditions for the 5.5 kVA salient pole synchronous generator a) with the rotor skew, b) without the rotor skew

In the presented waveforms (Fig. 18), the total harmonic distortion of the $u_{as}$ and $u_a$ (with and without the rotor skew) for the case of $U_f$ = const. are:

- for the 5.5 kVA synchronous generator with the rotor skew $THDu_{as}$ = 8.29%,
- for the 5.5 kVA synchronous generator without the rotor skew $THDu_a$ = 15.18%.

## 6. Conclusions

This paper presents the detailed process for determining the induced stator phase voltages whilst taking into account the circuital model of the low power salient pole synchronous generator with and without the rotor skew with damping circuits. This model is based on the self and mutual stator to rotor inductance distributions that are determined by means of the FEMM program. Based on the simulation studies, it can be concluded that in a steady state when powering the field winding from a DC voltage source due to the presence of the damping bars on the rotor:

- without the skew and due to rotor current derivatives (in damping bars and field current) the increase of harmonic content in induced stator voltages is significant and registered $THDu_a$ = 15.18% and simulated $THDu_a$ = 13.73%,
- with the skew reduces the influence of the rotor current derivatives (in damping bars and field current) on the increase of harmonic content in induced stator voltages and registered $THDu_a$ = 8.29% and simulated $THDu_a$ = 8.39%.

Due to the presence of the stator slots ($Q_s$) in the field current and in the damping bar, currents dominate mainly $Q_s$-th harmonic. As shown in this paper, for the examined 5.5 kVA synchronous generator, the current derivative $\mathrm{d}\mathbf{i}_r/\mathrm{d}t$ in same damping bars for 24th harmonic ($Q_s$ = 24) has a value of almost 11 kA/s. Although, the magnitude of the stator to damping bar (and part of the two rings) of the mutual inductance distributions $\mathbf{L}_{sr} = [L_{ar(1)}, \ldots, L_{ar(10)}; L_{br(1)}, \ldots, L_{br(10)}; L_{cr(1)}, \ldots, L_{cr(10)}]$ are equal to 0.4 mH, but the product of the $\mathbf{L}_{sr}\mathbf{di}_r/\mathrm{d}t$ has significant influence on the waveforms of the induced stator voltages for the model without a rotor skew.

The main advantages of the circuital modelling (in comparison with simulations using a field model) are the short calculation time, direct and complete control of the influence of every electromagnetic parameter on increasing or reduction of the harmonic contents in the induced stator phase voltages. In the case of a field model simulation of the salient pole synchronous generator with damping circuits with and without the rotor skew, it is difficult to determine which of the electromagnetic parameters have an influence on the induced stator phase voltages.

As shown in this article, FEMM cooperation (in determining the self and mutual inductance distributions) with numerical calculation of the inductance derivative distributions and the simulations in the circuital model give good results similar to experimental ones.

## References


[1] Keller S., Xuan M.T., Simond J.J., *Prediction of the no-load voltage waveform of laminated salient pole synchronous generators*, Industry Applications Conference, Fortieth IAS Annual Meeting, 2–6 Oct. 2005, Vol. 4, pp. 2265–2271.

[2] Keller S., Tu Xuan M., Simond J.J., *Computation of the no-load voltage waveform of laminated salient-pole synchronous generators*, IEEE Transactions on Industry Applications, 2006, Vol. 42, No. 306, pp. 681–687.

[3] Glinka T., *Synchronous generators used as reactive power compensators and higher harmonics filters*, Zeszyty Problemowe – Maszyny Elektryczne, 2013, nr 1, Komel, Katowice, pp. 51–62.

[4] May H., Palka R., Paplicki P., Szkolny S., Canders W.R., *Modified concept of permanent magnet excited synchronous machines with improved high-speed features*, Archives of Electrical Engineering, 2011, Vol. 60, No. 4, pp. 531–540.

[5] Skwarczyński J., Weinreb K., *Method of Analysis of Slot Harmonics in the Salient-Pole Synchronous Generators*, International Conference on Electrical Machines (ICEM), Boston, MA, 13–15 August, 1990, pp. 1165–1170.

[6] Vicol L., Banyai A., Viorel I.A., Simond J.J., *On the damper cage bars' currents calculation for salient pole large synchronous machines*, Advances in Electrical and Electronic Engineering, 2008, Vol. 7, No. 1, pp. 165–170.

[7] Moreira J., Lipo T.A., *Modeling of Saturated AC Machines Including Airgap Flux Harmonic Components*, IEEE-IAS Conference Record, 7–12 Oct., 1990, Part 1, pp. 37–44.
[8] Sobczyk T.J., *Mathematical model of synchronous generators accounting for saturation due to the first and the third MMF harmonic*, SME, OWPW, Elektryka, 1999, No. 111, pp. 42–51.
[9] Sobczyk T.J., *Methodology of mathematical modeling of induction machines*, WNT, Warsaw 2004.
[10] Skwarczyński J., *Salient poles inner asymmetries*, Scientific Bulletins of Stanisław Staszic Academy of Mining and Metallurgy, Electrotechnics, Bulletin 16, 1990.
[11] Weinreb K., Sułowicz M., Dziechciarz A., *Application of instantaneous power for rotor eccentricity detection in synchronous motor*, Zeszyty Problemowe – Maszyny Elektryczne, 2014, nr 104, Komel, Katowice, pp. 301–306.
[12] Weinreb K., Sułowicz M., *Noninvasive diagnostics of synchronous machine windings internal asymmetry*, Zeszyty Problemowe – Maszyny Elektryczne, 2007, nr 77, Komel, Katowice, pp. 59–64.
[13] Weinreb K., Węgiel T., Sułowicz M., *Influence of inside asymmetry in asynchronous motor on spectrum of stator currents*, Proceeding of XLII$^{nd}$ International Symposium on Electrical Machines, SME, 3–6 July, 2006, Cracow, Poland, pp. 307–310.
[14] Ludwinek K., *Influence of Representation of the Stator to Rotor Mutual Inductances on the Induced Phase Voltage Waveforms in a Salient Pole Synchronous Generator*, Zeszyty Problemowe – Maszyny Elektryczne, 2014, nr 104, Komel, Katowice, pp. 147–154.
[15] Ludwinek K., *Influence of DC voltage and current of field winding on induced stator voltages of a salient pole synchronous generator*, International Review of Electrical Engineering, 2014, Vol. 9, No. 1, pp. 62–72.
[16] Ludwinek K., *Representation of the mutual inductances in a circuital model of a salient-pole synchronous machine*, Elektro. Info, 2013, No. 9, pp. 103–111.
[17] Ludwinek K., *Representation of the stator to rotor self- and mutual inductances in a salient pole synchronous generator in the no-load state*, Zeszyty Problemowe – Maszyny Elektryczne, 2014, nr 104, Komel, Katowice, pp. 117–124.
[18] Ludwinek K., *An overview of the most important methods of reducing the harmonic content introduced by discretely distributed armature winding*, Elektro. Info, 2014, No. 7–8, pp. 53–57.
[19] Ludwinek K., *Some aspects of representation of inductance distributions in dq0-axes in a salient pole synchronous generator*, Zeszyty Problemowe – Maszyny Elektryczne, 2014, nr 104, Komel, Katowice, pp. 187–184.
[20] http://www.femm.info/wiki/HomePage.